

NMR and Neutron Scattering Studies of Quasi One-Dimensional Magnet CuV_2O_6

Jun KIKUCHI*, Kazuhiro ISHIGUCHI, Kiyoichiro MOTOYA, Masayuki ITOH¹,
Kazunori INARI², Naotoshi EGUCHI² and Jun AKIMITSU²

*Department of Physics, Faculty of Science and Technology, Science University of Tokyo,
2641 Yamazaki, Noda, Chiba 278-8510*

¹*Department of Physics, Faculty of Science, Chiba University,
1-33 Yayoi-cho, Inage-ku, Chiba 263-8522*

²*Department of Physics, College of Science and Engineering, Aoyama-Gakuin University,
6-16-1 Chitosedai, Setagaya-ku, Tokyo 157-8572*

(Received April 17, 2000)

Magnetic properties of a quasi one-dimensional magnet CuV_2O_6 have been studied by means of susceptibility measurement, NMR and powder neutron diffraction. Cu^{2+} spins ($S = 1/2$) order antiferromagnetically below 22.6 K, and the saturation moment is about $0.70 \mu_B$ at 0 K. The magnetic structure determined in the present study indicates that in CuV_2O_6 one-dimensional antiferromagnetic spin chains are along [110], suggesting a dominant antiferromagnetic exchange interaction between the next-nearest-neighbor spins rather than the nearest-neighbor ones.

KEYWORDS: CuV_2O_6 , NMR, neutron diffraction, low-dimensional magnet

§1. Introduction

A Heisenberg antiferromagnetic linear chain (HAFC) with $S = 1/2$ has attracted much attention because of its critical nature of the ground state. Quantum fluctuations in the $S = 1/2$ HAFC are so strong that the ground state is disordered and is gapless, and the spin-spin correlation function decays as a power law in an infinite correlation length. Because of its criticality, a small perturbation causes a drastic change of the ground state to the one with spontaneous broken symmetry. A coupling with phonons, for example, results in a new disordered ground state with an energy gap for the excitation channels, accompanying spontaneous dimerization of the spins. This is known as the spin-Peierls transition.¹⁾ An interchain coupling is also a trigger for transition to the three-dimensionally-ordered ground state with spontaneous sublattice magnetization, which is usually encountered in a lot of “quasi” one-dimensional materials.

An insulating copper vanadate CuV_2O_6 is one of the possible candidates of an $S = 1/2$ HAFC. CuV_2O_6 crystallizes in the triclinic structure of space group $P\bar{1}$ with lattice parameters $a = 9.168 \text{ \AA}$, $b = 3.543 \text{ \AA}$, $c = 6.478 \text{ \AA}$, $\alpha = 92.25^\circ$, $\beta = 110.34^\circ$ and $\gamma = 91.88^\circ$.^{2,3)} The structure consists of linear chains of edge-sharing CuO_6 octahedra along [010] or the b axis, bridged by VO_5 pyramids forming a zig-zag chain (or also viewed as double chains) of V atoms running along [010] as well (see Fig. 1). Valences of the ingredient atoms are Cu^{2+} , V^{5+} and O^{2-} , and the Cu^{2+} ion has a spin one half as only the magnetic constituent. The Cu-Cu distances are 3.543 \AA along [010], 4.860 \AA along [110], 4.968 \AA along $[1\bar{1}0]$ and 6.478 \AA along [001]. Because the distance between

Cu atoms is the shortest along [010] and there seems to be a relevant exchange path via the shared CuO_6 octahedral edge in that direction, one naively expects that CuV_2O_6 has one-dimensional (1D) chains of Cu^{2+} spins along [010] and that the magnetic properties can well be described in terms of an $S = 1/2$ HAFC. Indeed, a broad maximum of the magnetic susceptibility has been observed around 44 K,⁴⁾ which indicates strong short-range antiferromagnetic correlation between Cu^{2+} spins. On the other hand, it has been reported from the AFMR measurement that CuV_2O_6 has a long-range-ordered ground state below 23 K,⁴⁾ implying a relatively large interchain coupling.

Although the low-dimensional character of the spin system in CuV_2O_6 is evident from the preceding work,⁴⁾ it seems that the magnetic properties of CuV_2O_6 have not yet been well characterized because of the lack of microscopic experiments. It is therefore worthwhile to conduct an experiment on CuV_2O_6 such as the nuclear magnetic resonance (NMR) and the neutron diffraction. In this paper, we present results of magnetic susceptibility, NMR and powder neutron diffraction measurements on CuV_2O_6 . We confirmed that CuV_2O_6 exhibits commensurate antiferromagnetic ordering below the Néel temperature of 22.6 K. We unexpectedly found that the spin chains are ordered antiferromagnetically not along [010] but [110], corresponding to the direction of next-nearest neighbors for Cu, the origin of which will be argued based on the local electronic state of the Cu^{2+} ion.

§2. Experiments

Polycrystalline samples of CuV_2O_6 were prepared by the solid-state reaction of CuO and V_2O_5 . They were mixed in an alumina crucible and fired in air at 500°C . The firing and intermediate grinding were repeated un-

* E-mail: kikuchi@ph.noda.sut.ac.jp

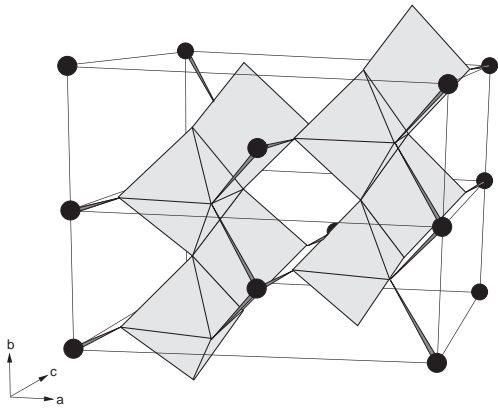


Fig. 1. Crystal structure of CuV_2O_6 . The solid circles are Cu atoms and the gray polyhedra represent VO_5 pyramids. Cu-O bonds are shown for oxygens shared by CuO_6 and VO_5 polyhedra.

til the impurity phases such as CuV_2O_7 were not detected by the powder X-ray diffraction measurement. The time in obtaining a single phase was totally of about 200 hours. Magnetic susceptibility was measured using a SQUID magnetometer (Quantum Design MPMS-5s) at 1.5 T. ^{51}V NMR spectra were taken by recording the spin-echo signals with a Box-car integrator while sweeping the external magnetic field at a fixed frequency. The Cu NMR spectrum was taken by recording the spin-echo signals under zero external field point by point of frequencies. Powder neutron-diffraction measurements were performed on the triple-axis spectrometer (T1-1) in a two-axis mode installed at JRR-3M in JAERI at Tokai. Pyrolytic graphite monochromator and filter were used to select the incident neutrons. The wave number of incident neutrons was 2.575 \AA^{-1} and the horizontal beam collimation, $7'-40'-40'-40'$, was used in the experiments.

§3. Results and Analysis

3.1 Magnetic Susceptibility

The temperature dependence of the magnetic susceptibility of CuV_2O_6 is shown in Fig. 2. The susceptibility exhibits a broad maximum around $T_{\text{max}} \approx 48 \text{ K}$ which is characteristic of low-dimensional system with antiferromagnetic interactions. Above T_{max} , the susceptibility can well be fitted to the Bonner-Fisher curve for the $S = 1/2$ HAFC.⁵⁾ In order to estimate the intrachain exchange coupling J between Cu^{2+} spins, we fitted the temperature (T) dependence of the susceptibility χ to the following formula;⁶⁾

$$\chi = \chi_0 + \frac{N_A g^2 \mu_B^2}{k_B T} \times \frac{0.25 + 0.14995x + 0.30094x^2}{1 + 1.9862x + 0.68854x^2 + 6.0626x^3}. \quad (3.1)$$

Here χ_0 is a T independent part of χ , N_A is Avogadro's number, μ_B is the Bohr magneton and $x = J/k_B T$. From the least-squares fit of the data above 40 K, we obtained $\chi_0 = 3.5 \times 10^{-4} \text{ emu/mol}$, $g = 2.0$ and $J/k_B = 36 \text{ K}$. A relatively large value of χ_0 may be attributed to Van-Vleck orbital paramagnetism of Cu^{2+} ions. As the tem-

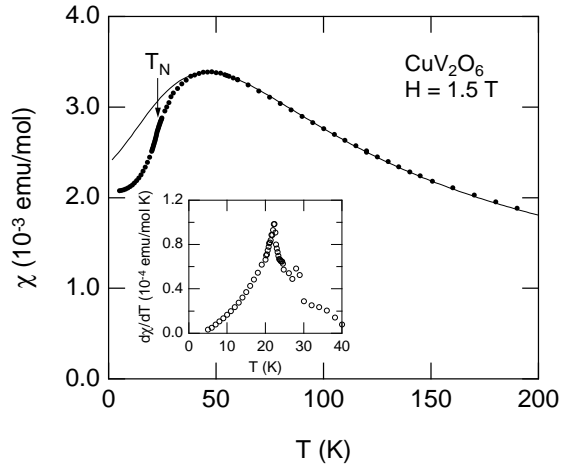


Fig. 2. Temperature dependence of the magnetic susceptibility of CuV_2O_6 . Néel temperature is indicated by an arrow. The solid line is a fit of the data above 40 K to the susceptibility of an $S = 1/2$ Heisenberg antiferromagnetic linear chain. The inset shows $d\chi/dT$ which exhibits a sharp peak at T_N .

perature is decreased below T_{max} , the observed χ begins to deviate from the Bonner-Fisher curve. This is considered to be a crossover to higher dimensions resulting from the interchain coupling. Indeed, long-range antiferromagnetic ordering takes place below 22.6 K as will be shown below.

Although we cannot see a clear anomaly in the $\chi - T$ curve indicative of long-range magnetic ordering, we observed a sharp peak in the temperature derivative of the susceptibility $d\chi/dT$ at 22.4 K as shown in the inset of Fig. 2. It is reasonable to consider that the anomaly is due to the long-range magnetic ordering of Cu^{2+} spins.

3.2 ^{51}V NMR

Figure 3 shows the field-swept NMR spectrum at various temperatures taken at an NMR frequency of 16.5 MHz. The spectra exhibit powder patterns which distribute around the zero-shift position for ^{51}V nuclei. The fine structure in the spectrum observed above 22.6 K can be assigned as singularities resulting from the electric quadrupole interaction for nuclei with a nuclear spin $I = 7/2$. We therefore conclude that the observed signal comes from ^{51}V nuclei ($I = 7/2$) on the nonmagnetic V site.

The spectrum starts to be broadened suddenly below 22.6 K to have a rectangular shape with the center of gravity near the unshifted resonance position for ^{51}V . The broadening evidences long-range magnetic ordering of Cu^{2+} spins giving rise to a finite internal magnetic field at the V site. The rectangular shape of the spectrum is typical for nonmagnetic nuclear sites in the antiferromagnet with the internal field much smaller than the applied one. The line shape also indicates a commensurate antiferromagnetic structure in which all the V sites feel a unique internal-field strength from Cu^{2+} spins.

In order to determine the magnitude of the internal

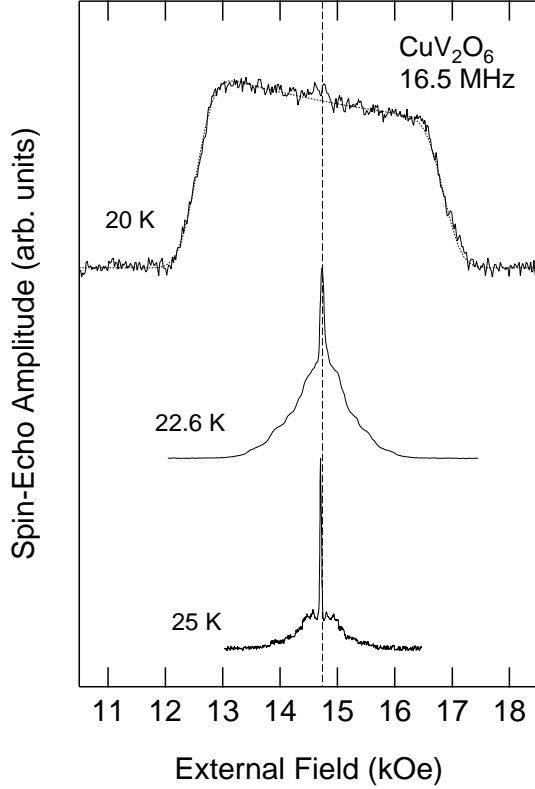


Fig. 3. Temperature variation of the field-swept NMR spectrum of ^{51}V in CuV_2O_6 taken at 16.5 MHz. The dashed line indicates a position of zero shift for ^{51}V . The dotted line is a fit of the experimental data at 20 K to eq. (3.2) broadened by an inhomogeneous distribution of the internal field.

field H_n at the V site which is proportional to the sublattice magnetization,⁷⁾ we calculated the line shape of the NMR spectrum in the antiferromagnetic state and fitted the observed spectrum to the calculated one. Details of the derivation and the fitting procedure should be referred to the appendix. We describe here an essence of the calculation. For a powder sample in which a direction of the internal field is randomly distributed with respect to that of the applied field H , the NMR spectrum $f(H)$ as a function of H has the following form;

$$f(H) \propto \frac{H^2 - H_n^2 + \omega^2/\gamma^2}{H_n H^2}. \quad (3.2)$$

Here ω is an NMR frequency which is assumed to be larger than γH_n (γ being the nuclear gyromagnetic ratio). The spectrum has two cutoff fields, $\omega/\gamma + H_n$ and $\omega/\gamma - H_n$, resulting in the sharp edges in the spectrum, which are usually smeared by an inhomogeneous distribution of the internal field present in a real crystal. We take account of this effect by assuming a gaussian distribution function for H_n . The result of the fit is shown in Fig. 3 by the dotted line. The quality of the fit is quite good and the magnitude of the internal field at 20 K was determined as $H_n = 2.15 \pm 0.06$ kOe.

The T dependence of the internal field at the V site is shown in Fig. 4. The internal field becomes nonzero below about 23 K and saturates to a value of about 3.1 kOe

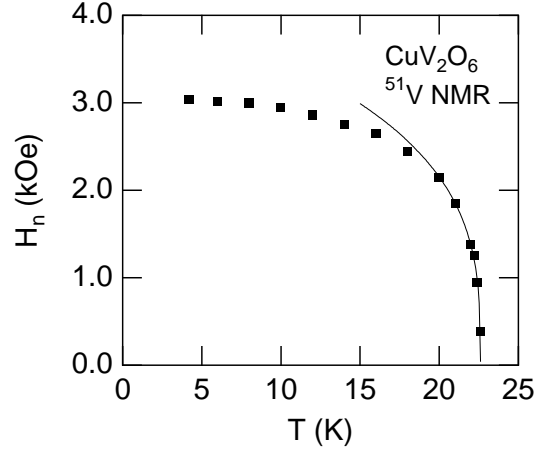


Fig. 4. Temperature dependence of the internal magnetic field at the V site in CuV_2O_6 . The solid line is a fit of the data above 20 K to the form $H_n \propto (1 - T/T_N)^\beta$ with $T_N = 22.60$ K and $\beta = 0.31$.

at $T = 0$ K. The Néel temperature T_N was determined by fitting H_n to be proportional to $(1 - T/T_N)^\beta$ near T_N , where β is the critical exponent for sublattice magnetization. From the least-squares fit of the data above 20 K, we obtained $T_N = 22.60 \pm 0.05$ K and $\beta = 0.31 \pm 0.01$. The exponent is close to those for three-dimensional (3D) magnetic systems,⁸⁾ suggesting the 3D nature of magnetic ordering.

In the paramagnetic state above T_N , the ^{51}V NMR spectrum exhibits a powder pattern resulting from the anisotropy of NMR shift and electric-field gradient (EFG) at the V sites. All the peaks and shoulders observed in the satellites can be assigned as singularities which appear when the external magnetic field is parallel to one of the principal axes of the EFG tensor. By analyzing the positions of peaks and shoulders in the satellites, one can determine the tensor components of the NMR shift, and the EFG parameters such as the nuclear quadrupolar frequency ν_Q and the asymmetric parameter η .⁹⁾ Taking account of the quadrupolar effect on the Zeeman interaction as a perturbation up to second order, we determined the NMR shifts and the EFG parameters at each temperature. The results are shown in Figs. 5 and 6.

Due to low point symmetry, the EFG at the V sites is rather asymmetric with an η value of 0.45 – 0.51 which depends weakly on temperature. As a V^{5+} ion has no valence electron, the EFG at the V site is mainly determined by the contribution from surrounding lattice ions which may be regarded as point charges. The lattice contribution to the EFG evaluated in terms of the point-charge model yields η of 0.51 at room temperature, which agrees well with the experiment. This suggests that the large asymmetry of the EFG at the V site results from the asymmetric configuration of surrounding lattice ions.

The NMR shifts K_μ ($\mu = X, Y$ and Z) exhibit a broad maximum around 50 K, corresponding to the bulk χ as shown in Fig. 6. A standard $K - \chi$ analysis indi-

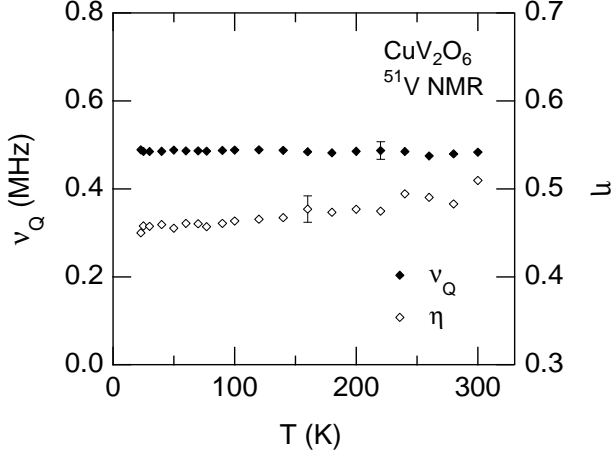


Fig. 5. Temperature dependence of the nuclear quadrupolar frequency ν_Q and the asymmetric parameter η at the V site in CuV_2O_6 . Error bars are shown for some data points.

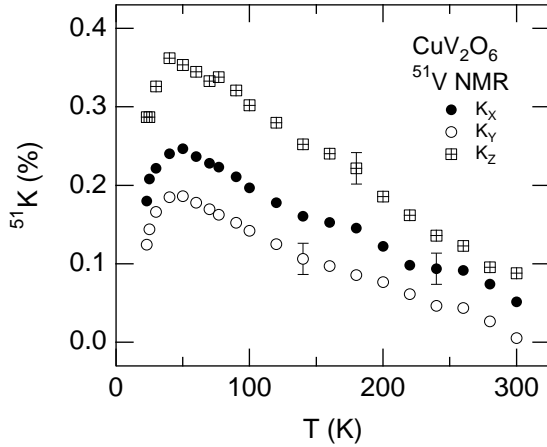


Fig. 6. Temperature dependence of the NMR shift at the V site in CuV_2O_6 . Error bars are shown for some data points.

cated that K_μ 's are proportional to χ . From the proportionality constants between K_μ 's and χ , we determined the tensor components of the hyperfine interaction at the V site along the μ principal axes of the EFG as $A_X = 4.7 \pm 0.2 \text{ kOe}/\mu_B$, $A_Y = 4.3 \pm 0.2 \text{ kOe}/\mu_B$ and $A_Z = 7.0 \pm 0.3 \text{ kOe}/\mu_B$. A_μ 's are relatively large for nuclei on the nonmagnetic site which indicates finite spin transfer from neighboring Cu^{2+} spins. It should also be noted that the hyperfine tensor is anisotropic. One of the origins of an anisotropy in the hyperfine tensor is the classical dipolar field from surrounding electronic spins, which can be evaluated numerically if we know the atomic positions of both V and Cu. Based on the given lattice parameters,²⁾ we calculated the classical dipolar field at the V site along the lattice EFG principal axes to be $A_X^{\text{dip}} = 0.26 \text{ kOe}/\mu_B$, $A_Y^{\text{dip}} = -0.67 \text{ kOe}/\mu_B$ and $A_Z^{\text{dip}} = 0.45 \text{ kOe}/\mu_B$. Since the observed hyperfine coupling constants can be expressed as $A_\mu =$

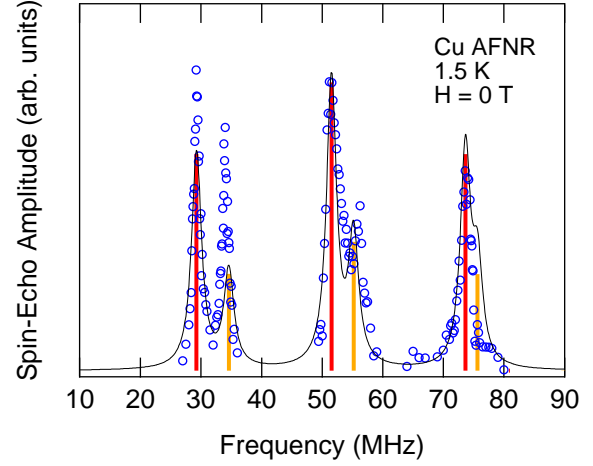


Fig. 7. The zero-field NMR spectrum of Cu in CuV_2O_6 taken at 1.5 K. The data points are shown by open circles. The vertical lines indicate resonance frequencies and intensities for ^{63}Cu (black) and ^{65}Cu (gray) nuclei calculated using parameters; $H_n = 4.56 \text{ T}$, $^{63}\nu_Q = 22.2 \text{ MHz}$ and $\eta = 0.32$. The solid line is a simulation of the NMR spectrum based on the calculated resonance frequencies and intensities broadened by a Lorentzian width of 1.0 MHz.

$A_\mu^{\text{tr}} + A_\mu^{\text{dip}}$, the anisotropy of the transferred hyperfine coupling (A_μ^{tr}) can be obtained by subtracting the dipolar coupling from the observed one. We then obtained the following values of the transferred hyperfine coupling; $A_X^{\text{tr}} = 4.4 \pm 0.2 \text{ kOe}/\mu_B$, $A_Y^{\text{tr}} = 5.0 \pm 0.2 \text{ kOe}/\mu_B$ and $A_Z^{\text{tr}} = 6.5 \pm 0.3 \text{ kOe}/\mu_B$. Although the transferred hyperfine coupling is dominated by the isotropic part $A_{\text{iso}}^{\text{tr}} = \frac{1}{3}\sum_\mu A_\mu^{\text{tr}} = 5.3 \pm 0.7 \text{ kOe}/\mu_B$, it has a finite anisotropy not due to the classical dipolar field. This suggests that the anisotropic orbital such as $2p$, $3p$ and $3d$ orbitals on V atoms are polarized by spin transfer from neighboring Cu atoms.

3.3 Cu NMR

We observed an NMR of Cu nuclei under zero external magnetic field well below T_N , which again confirms long-range magnetic ordering. Figure 7 shows the zero-field NMR spectrum of Cu taken at 1.5 K. No signal is observed except the observed one in a frequency range from 20 to 100 MHz. The observed five resonance lines are signals from the two isotopes, ^{63}Cu and ^{65}Cu , which both have nuclear spin I of $3/2$, split by the electric quadrupolar interaction. The absence of one of the six lines expected in the presence of the quadrupolar interaction is due to an accidental overlap of satellite lines of the two isotopes.

In order to determine the internal magnetic field H_n , the quadrupolar frequency ν_Q and the asymmetric parameter η at the Cu site, we calculated energy levels of a nuclear spin with $I = 3/2$ by solving a secular equation of the nuclear Hamiltonian of nuclear Zeeman and electric quadrupole interactions. This is because a perturbation theory cannot be applied to calculate energy levels and resonance frequencies in the present case where the relative strength of Zeeman and quadrupole interactions is

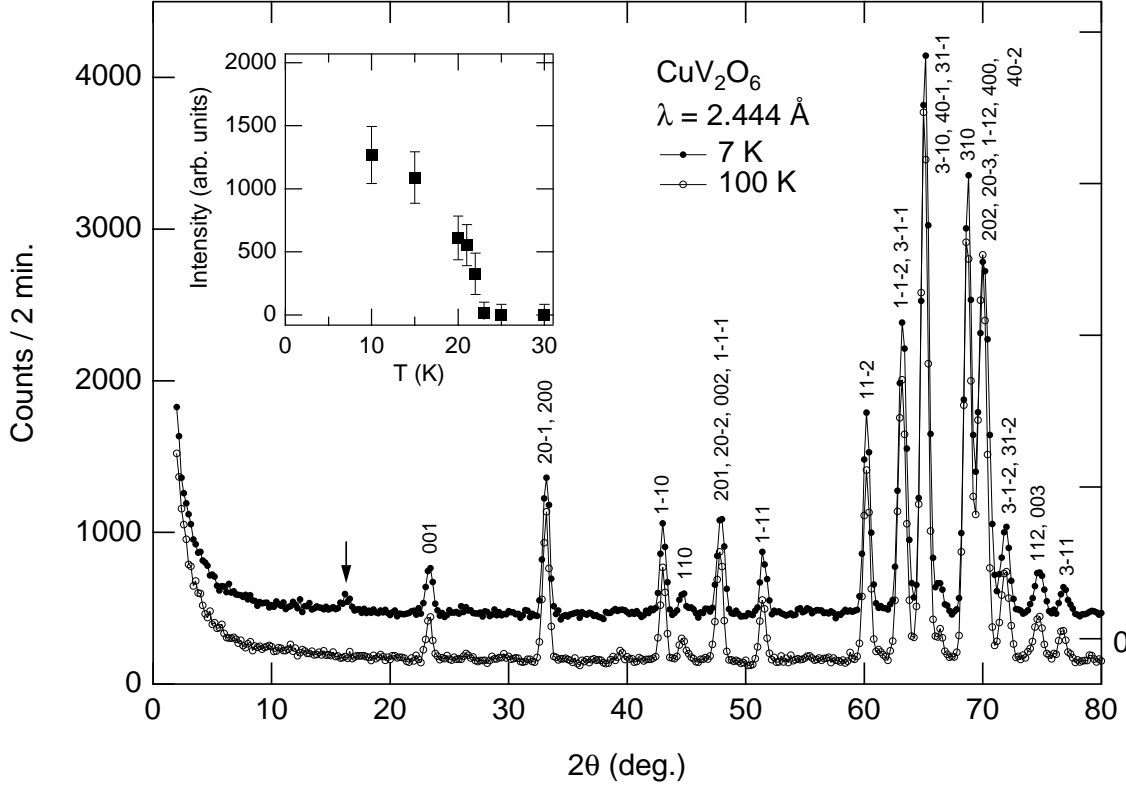


Fig. 8. Powder neutron diffraction patterns from CuV_2O_6 at 7 (offset by 300 counts) and 100 K. The inset shows temperature dependence of the integrated intensity of the Bragg peak with the scattering angle 2θ of 16.3° . An arrow indicates the magnetic Bragg peak.

unknown and may be comparable in magnitude. The Hamiltonian for Cu nuclei is generally written as

$$\mathcal{H} = -\gamma\hbar\mathbf{I} \cdot \mathbf{H}_n + \frac{\hbar\nu_Q}{6}[3I_z^2 - I(I+1) + \frac{\eta}{2}(I_+^2 + I_-^2)]. \quad (3.3)$$

The first and second terms are the nuclear Zeeman and electric quadrupolar interactions, respectively, and the coordinate refers to the principal axes of the EFG tensor. γ is the nuclear gyromagnetic ratio ($^{63}\gamma = 11.285 \text{ MHz/T}$ and $^{65}\gamma = 12.089 \text{ MHz/T}$), \hbar is Planck's constant, \mathbf{H}_n is the internal magnetic field and \mathbf{I} is the nuclear spin operator. When a direction of the internal magnetic field is parallel to one of the principal axes of the EFG tensor, the Hamiltonian (3.3) can be diagonalized analytically, so that the energy levels and the transition probabilities between them can be obtained in an analytical form. On the assumption that the internal magnetic field is along either X , Y or Z axis of the EFG tensor, we tried to reproduce the observed resonance frequencies by tuning parameters $H_n = |\mathbf{H}_n|$, $^{63}\nu_Q$ and η .¹⁰⁾ A good fit was obtained when the direction of the internal field is along the Z axis of the EFG tensor. The obtained parameters are $H_n = 4.56 \text{ T}$, $^{63}\nu_Q = 22.2 \text{ MHz}$ and $\eta = 0.32$, which were used to simulate the NMR spectrum shown by the solid line in Fig. 7.

3.4 Powder Neutron Diffraction

Our NMR experiments presented above confirmed long-range magnetic ordering of Cu^{2+} spins in CuV_2O_6 . However, the magnetic structure can hardly be determined from NMR on powder specimens. We therefore performed a powder neutron diffraction measurement on CuV_2O_6 .

Figure 8 shows the powder diffraction patterns from CuV_2O_6 at 7 and 100 K. At 7 K ($< T_N$), a new peak appears at the scattering angle of $2\theta = 16.3^\circ$. As shown in the inset of Fig. 8, the peak disappears above T_N and is confirmed to be magnetic in origin. In table I, we summarized the scattering angle and intensity of the observed peaks at 10 K and 30 K along with the Miller indices based on the chemical unit cell. Within experimental accuracies, there is no magnetic reflection except the observed one.

The magnetic reflection appeared at $2\theta = 16.3^\circ$ can be indexed as either (100) or $(10\frac{1}{2})$ on the basis of the original triclinic cell. We cannot make a unique determination of the magnetic structure because no other magnetic peak was found. Possible antiferromagnetic structures which produce either (100) or $(10\frac{1}{2})$ magnetic reflection are shown schematically in Fig. 9. The structure (A) corresponds to the reflection (100) and the structure (B) to the reflection $(10\frac{1}{2})$.

Table I. The observed Bragg angles and intensities of scattered neutrons at 10 and 30 K in CuV_2O_6 . The intensities are normalized to 1000 at the Bragg angle of 65.13° . Errors in the Bragg angles are within 0.05° . Large errors in I_{obs} are due to incoherent scattering of neutrons by vanadium.

10 K		30 K		hkl
$2\theta_{\text{obs}}$	I_{obs}	$2\theta_{\text{obs}}$	I_{obs}	
16.27	19 ± 8	—	—	100 or $10\frac{1}{2}$
23.38	78 ± 8	23.35	71 ± 8	001
33.18	244 ± 9	33.17	241 ± 10	200, $20\bar{1}$
43.03	138 ± 8	43.03	140 ± 9	$1\bar{1}0$
44.65	41 ± 9	44.63	37 ± 10	110
47.90	191 ± 9	47.89	196 ± 9	201, $20\bar{2}$, 002, $1\bar{1}\bar{1}$
51.52	102 ± 7	51.53	100 ± 9	$1\bar{1}\bar{1}$
60.22	314 ± 13	60.22	306 ± 12	$11\bar{2}$
63.27	548 ± 19	63.26	566 ± 19	$1\bar{1}\bar{2}$, $3\bar{1}\bar{1}$
65.13	1000	65.13	1000	$40\bar{1}$, $31\bar{1}$, $3\bar{1}0$
68.74	754 ± 17	68.73	766 ± 17	310
70.07	915 ± 22	70.06	887 ± 22	$1\bar{1}\bar{2}$, $40\bar{2}$, $20\bar{3}$, 400, 202
71.91	170 ± 11	71.90	172 ± 19	$31\bar{2}$, $3\bar{1}\bar{2}$
74.78	100 ± 11	74.78	92 ± 11	112, 003
76.89	56 ± 9	76.85	55 ± 15	$3\bar{1}\bar{1}$
82.00	374 ± 19	81.99	383 ± 20	$11\bar{3}$, 311
84.32	282 ± 12	84.30	284 ± 21	$40\bar{3}$, 401
86.26	73 ± 21	86.19	56 ± 23	$1\bar{1}\bar{3}$
87.26	663 ± 26	87.24	672 ± 25	020, $31\bar{3}$
89.89	22 ± 16	89.79	18 ± 17	$3\bar{1}\bar{3}$

It is surprising that in both magnetic structures, the nearest-neighbor spins align *ferromagnetically*. The anti-ferromagnetic alignment of the spins is commonly found along $[110]$ (or $[1\bar{1}0]$), which is the direction of the next-nearest-neighbor sites of Cu. It should be noted that the broad maximum of the susceptibility and the negative Weiss temperature obtained from the high-temperature region indicate a dominant antiferromagnetic coupling between Cu^{2+} spins. This suggests that the exchange coupling between the next-nearest neighbors is stronger than that between the nearest neighbors. The antiferromagnetic spin chains in CuV_2O_6 are considered to be along $[110]$ (or $[1\bar{1}0]$) rather than $[010]$, which is not readily speculated from the crystal structure.

By symmetry, both (100) and $(10\frac{1}{2})$ reflections are purely magnetic in origin, and the intensity I_{hkl} of scattered neutrons is proportional to the square of the magnetic structure factor F_{m}^{hkl} as $I_{hkl} \propto \langle q^2 \rangle |F_{\text{m}}^{hkl}|^2$.¹¹⁾ F_{m}^{hkl} is proportional to the thermal average of the magnetic moment $\langle \mu \rangle$ and $\langle q^2 \rangle$ is a geometrical factor depending on the orientation of the magnetic moment with respect to the scattering vector.¹²⁾ $\langle q^2 \rangle$ is given for the (100) reflection as

$$\langle q^2 \rangle = 1 - d_{100}^2 a^{*2} \cos^2 \varphi_a, \quad (3.4a)$$

and for $(10\frac{1}{2})$,

$$\langle q^2 \rangle = 1 - d_{10\frac{1}{2}}^2 (a^* \cos \varphi_a - \frac{c^*}{2} \cos \varphi_c)^2. \quad (3.4b)$$

Here d_{hkl} is the spacing of (hkl) planes, a^* and c^* are lattice constants in reciprocal space, φ_a and φ_c are angles between the direction of the magnetic moment and the a

and c axes, respectively. As we have only one magnetic reflection that is observable, we cannot determine the angles φ_a , φ_c , and $\langle \mu \rangle$ only from the neutron diffraction data. Fortunately, we know from the Cu NMR that the moment is along the Z principal axis of the EFG tensor at the Cu site, the direction of which can be evaluated from the symmetry of the EFG due to surrounding lattice ions.¹³⁾ The point-charge calculation of the lattice EFG at the Cu site yields the angles $\varphi_a = 109^\circ$ and $\varphi_c = 100^\circ$ between the Z principal axis of the EFG and the crystalline a and c axes, respectively. The calculation also yields the angle $\varphi_b = 23^\circ$ between the Z principal axis of the EFG and the b axis, specifying the direction of the magnetic moment with respect to all the crystalline axes. For this direction of the magnetic moment ($\parallel Z$), the intensity of the (010) reflection at $2\theta = 40.4^\circ$ allowed for the structure (A) is order-of-magnitude smaller than that of (100) . This is why the fundamental (010) reflection could not be observed in the present experiment. Using the calculated values of φ_a and φ_c , and the magnetic form factor of the free Cu^{2+} ion¹⁴⁾ for F_{m}^{hkl} , $\langle \mu \rangle$ at 10 K is determined to be $0.69 \pm 0.07 \mu_B$ for (100) and $0.67 \pm 0.07 \mu_B$ for $(10\frac{1}{2})$. The saturation moment at 0 K is then evaluated to be $0.72 \pm 0.07 \mu_B$ and $0.70 \pm 0.07 \mu_B$ for (100) and $(10\frac{1}{2})$, respectively, with the aid of the T dependence of the internal magnetic field at the ^{51}V site (Fig. 10). The extrapolated values of $\langle \mu \rangle$ at 0 K are slightly smaller than that expected in the 3D-ordered antiferromagnet with $S = 1/2$,¹⁵⁾ which may be attributed to the low-dimensionality of the present compound.

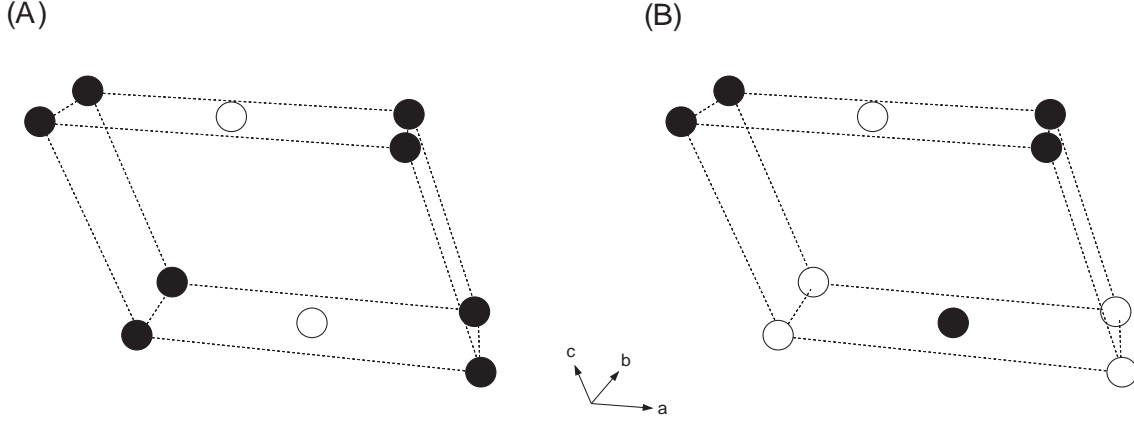


Fig. 9. Two possible magnetic structures in CuV_2O_6 which produce (A) (100) and (B) $(10\frac{1}{2})$ magnetic reflections, respectively. Only the Cu atoms are shown. Up and down spins are represented by the open and solid circles, respectively.

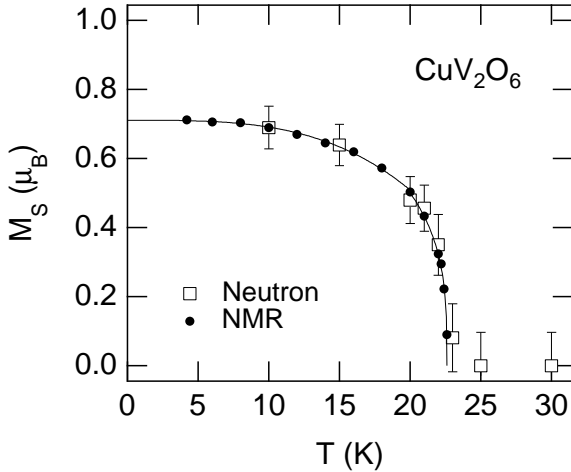


Fig. 10. Temperature dependence of the magnetic moment on Cu atoms in CuV_2O_6 . The solid line is a guide to the eyes. The moment is calculated for the magnetic structure (A). The neutron and NMR data are scaled to match at 10 K, yielding the hyperfine coupling constant in the antiferromagnetic state $|A_{hf}^{AF}| = 4.3 \text{ kOe}/\mu_B$. For the structure (B), the vertical axis should be rescaled by multiplying a factor of 0.965.

§4. Discussion

One of the important points to be discussed here is the magnetic structure of CuV_2O_6 revealed by the present neutron-diffraction measurements. The antiferromagnetic alignment of Cu^{2+} spins is found not along [010] (or b axis) which we thought as the direction of the 1D spin chain, but in the ab plane probably because of the dominant next-nearest-neighbor coupling. The ab plane antiferromagnetism might suggest two-dimensional (2D) coupling of Cu^{2+} spins rather than the 1D one along either [110] or $[1\bar{1}0]$, and is to be examined as well. In this section, we discuss possible exchange paths between Cu^{2+} spins based on the crystal structure and show that the 1D spin chain is likely to be along [110].

The magnetic structure of CuV_2O_6 can be understood by examining the local symmetry at the Cu site. Although the atomic site of Cu has only inversion symmetry, the electronic state of a Cu^{2+} ion may be derived from the approximate tetragonal symmetry. In the CuV_2O_6 structure, each Cu atom is surrounded by six oxygen atoms which make a distorted octahedron. The first and second nearest neighbors of the six oxygens are the O(1) and O(2) sites forming a parallelogram with the Cu atom in the center of gravity. The distortion of this parallelogram from a square is very small, because the sides differ by only 1.6 % (2.774 Å and 2.819 Å) and the two diagonals O(1)-Cu-O(1) and O(2)-Cu-O(2) make nearly a right angle ($\angle[\text{O}(1)\text{-Cu-O}(2)] = 89^\circ$ at room temperature). The octahedron is elongated with two apical oxygens on another O(2) sites, shared by the neighboring CuO_6 octahedra in the b direction as one of the “planar” oxygens. The line O(2)-Cu-O(2) is canted by 14° from the normal to the plane of the O(1) and O(2) parallelogram.

If we disregard these distortions and an effect of more distant atoms for qualitative discussion, the Cu site has tetragonal symmetry in an elongated octahedral environment, and the Cu^{2+} ion has one hole in the $d_{x^2-y^2}$ orbital state pointing toward the “planar” oxygens on the O(1) and O(2) sites. The relatively weak exchange between the nearest-neighbor Cu^{2+} spins can readily be understood because there is no relevant orbital to the exchange along [010] (there are negligible electronic densities pointing toward the “apical” oxygens). It should be noted that the tetragonal symmetry imposes the EFG at the Cu site to be symmetric about an axis of elongation (or $\eta = 0$). The modest asymmetry of the EFG at the Cu site ($\eta = 0.32$) evaluated from the present NMR experiment suggests that the deviation from tetragonal symmetry is not very large.

The $d_{x^2-y^2}$ -like character of the electronic state and the linkage of the CuO_6 octahedra favor the exchange along [110], excluding a possibility of 2D antiferromagnetism in the ab plane with comparable exchange inter-

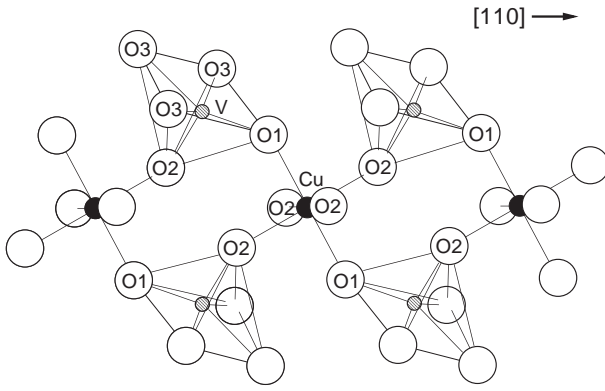


Fig. 11. The suggested Cu chain running along $[110]$ viewed from the apical oxygens of CuO_6 octahedra. Copper, vanadium and oxygen atoms are represented by solid, hatched and open circles, respectively. For some oxygen atoms, the site indices are explicitly shown. The CuO_6 octahedra are bridged by the two VO_5 pyramids successively to make a one-dimensional chain of Cu atoms along $[110]$.

actions in both $[110]$ and $[1\bar{1}0]$ directions. In the $[110]$ direction, the CuO_6 octahedra are bridged by two VO_5 pyramids which share the “planar” O(1) and O(2) sites of the CuO_6 octahedra as a corner and an apex of the VO_5 pyramid, respectively. This is shown schematically in Fig. 11. Since the $d_{x^2-y^2}$ orbital is in the plane of the O(1) and O(2) parallelogram, it may be possible that Cu^{2+} spins have an exchange coupling in the $[110]$ direction using the bridging VO_5 pyramids via the Cu-O-O-Cu path and/or Cu-O-V-O-Cu path. The anisotropic hyperfine tensor at the V site not due to the classical dipolar field seems to be consistent with such exchange paths through the VO_5 pyramids. On the other hand, there is no such linkage of the CuO_6 octahedra in the $[1\bar{1}0]$ direction. Therefore, the exchange along $[1\bar{1}0]$ is considered to be much weaker than that along $[110]$. This suggests that the antiferromagnetic spin chains in CuV_2O_6 are along $[110]$.

The distortion from ideal tetragonal symmetry results in the admixture of the other $3d$ states such as the d_{z^2} orbital pointing toward the apical oxygens, which enables Cu^{2+} spins to couple along the b axis. This is considered to be an origin of long-range magnetic ordering at non-zero temperature. The interchain coupling J' may be evaluated using the expression¹⁶⁾

$$\frac{T_N}{J} = \sqrt{\frac{z|J'|}{2J}}, \quad (4.1)$$

where z is the number of nearest-neighbor chains. Substituting $T_N = 22.6$ K, $J = 36$ K and $z = 2$ into eq. (4.1), we obtain $|J'| = 14$ K. Since the interchain coupling is considered to be ferromagnetic, J' may be negative and thus $J' = -14$ K.¹⁷⁾ A similar value of J' has been obtained in the previous report,⁴⁾ although a different formula is used for the estimation. A relatively large value of $|J'|$ compared with J indicates poor one dimensionality of the present system, which may be the origin of a relatively high ordering temperature.

§5. Conclusion

We have measured the susceptibility, NMR and powder neutron diffraction in an $S = 1/2$ quasi one-dimensional magnet CuV_2O_6 . It was confirmed that CuV_2O_6 exhibits three-dimensional antiferromagnetic ordering at the Néel temperature of 22.6 K, which is not far below the rounded maximum of the susceptibility observed around 48 K. The two possible antiferromagnetic structures were suggested and the saturation moments were evaluated to be 0.72 and 0.70 μ_B for the respective magnetic structures. The intra- and interchain couplings were also estimated to be 36 and -14 K, respectively.

The magnetic structure of CuV_2O_6 indicates that the exchange coupling between Cu^{2+} spins is stronger in the direction of next-nearest neighbors than in the direction of nearest neighbors. The origin of such exchange couplings was argued based on the local symmetry at the Cu site and the linkage of the CuO_6 octahedra in the crystal structure. It is suggested that the $d_{x^2-y^2}$ -like character of the electronic state inferred from symmetry is responsible for the relatively weak exchange between the nearest-neighbors spins along the b axis. A dominant antiferromagnetic exchange compatible with the $d_{x^2-y^2}$ -like orbital character may be the one acting via the Cu-O-O-Cu interaction paths, suggesting one-dimensional chains of Cu^{2+} spins along $[110]$. Because of such distant exchange paths for the intrachain coupling, CuV_2O_6 has a relatively large ratio of the interchain coupling to the intrachain one, which makes the Néel temperature of this compound relatively high.

Appendix: Field-swept NMR spectrum in the antiferromagnetic state

In this appendix, we will derive a powder pattern of the field-swept NMR spectrum in the antiferromagnetic state. In the presence of both internal magnetic field \mathbf{H}_n and external magnetic field \mathbf{H} , the resonance condition for a given nucleus is expressed as

$$\omega/\gamma = |\mathbf{H} + \mathbf{H}_n|. \quad (\text{A} \cdot 1)$$

This can be written alternatively as

$$\omega^2/\gamma^2 = H^2 + H_n^2 + 2HH_n \cos \theta, \quad (\text{A} \cdot 2)$$

where $H = |\mathbf{H}|$, $H_n = |\mathbf{H}_n|$ and θ is the angle between \mathbf{H} and \mathbf{H}_n . For a powder sample, the direction of \mathbf{H} is randomly distributed with respect to \mathbf{H}_n . The probability of \mathbf{H} and \mathbf{H}_n making an angle between θ and $\theta + \Delta\theta$ is proportional to the solid angle $\Delta\Omega \propto \sin\theta\Delta\theta$. The number of nuclei $\Delta N \equiv f(H)\Delta H$ such that the resonance field has a value between H and $H + \Delta H$ is proportional to $\Delta\Omega$ or $f(H)\Delta H \propto \sin\theta\Delta\theta$, giving the NMR line shape $f(H)$;

$$f(H) \propto \sin\theta \frac{d\theta}{dH}. \quad (\text{A} \cdot 3)$$

$d\theta/dH$ can be calculated by differentiating eq. (A·2). Substituting $d\theta/dH$ into eq. (A·3) yields

$$f(H) \propto \frac{H^2 - H_n^2 + \omega^2/\gamma^2}{H_n H^2}. \quad (\text{A} \cdot 4)$$

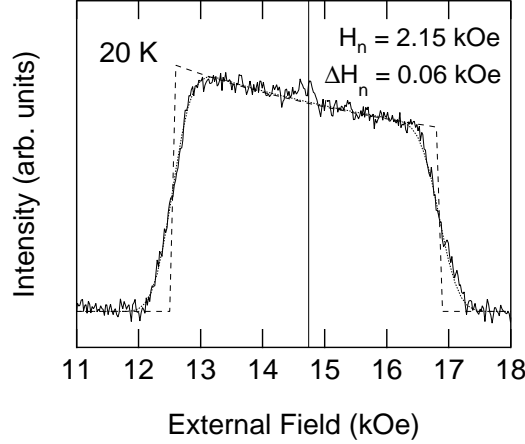


Fig. 12. Comparison of the calculated powder patterns and the observed ^{51}V NMR spectrum in CuV_2O_6 at 16.5 MHz and 20 K. The dashed line is the spectrum with no inhomogeneous broadening, eq. (A.4), showing sharp edges at $\omega/\gamma \pm H_n$. ω/γ corresponds to the zero-shift position for ^{51}V nuclei which is represented by the vertical line. The edges are equally spaced about ω/γ by H_n giving the spectral width of $2H_n$. The dotted line is a fit of the experimental data to eq. (A.5) for which the distribution function $g(H') \propto \exp(-\frac{1}{2} \frac{(H' - H_n)^2}{\Delta H_n^2})$ is assumed. The least-squares fit gives $H_n = 2.15$ kOe and $\Delta H_n = 0.06$ kOe at 20 K.

$f(H)$ is zero outside the region $\omega/\gamma - H_n \leq H \leq \omega/\gamma + H_n$ because $0 \leq \theta \leq \pi$. The spectrum is therefore cutoff at fields $\omega/\gamma \pm H_n$. In fact, an inhomogeneous distribution of H_n present in a real crystal broadens the spectrum (A.4), so that the sharp edges at the cutoff fields are obscured. The spectrum to be observed in the presence of an inhomogeneous broadening is now given by the convolution of eq. (A.4) and the distribution function $g(H')$ for H_n as

$$F(H) = \int f(H - H')g(H')dH'. \quad (\text{A.5})$$

As one usually assumes, we used a gaussian distribution function for $g(H')$ to reproduce ^{51}V NMR spectra in the antiferromagnetic state. In Fig. 12 we showed the results of the fit and an “ideal” spectrum with no inhomogeneous broadening (corresponding to the case $g(H') = \delta(H')$). From the least-squares fit of the data, we obtained $H_n = 2.15$ kOe at 20 K. The standard deviation of H_n was 0.06 kOe at 20 K which was taken to be the error in evaluating H_n .

- [7] V. Jaccarino: *Magnetism II A*, eds. G. T. Rado and H. Suhl, p.307 (Academic Press, New York, 1965).
- [8] For example, L. J. de Jongh and A. R. Miedema: *Experiments on Simple Magnetic Model Systems* (Taylor and Francis, London, 1974).
- [9] A. Abragam: *Principles of Nuclear Magnetism* (Oxford University Press, Oxford, 1961).
- [10] The quadrupole frequency $^{65}\nu_Q$ for ^{65}Cu is calculated from the isotopic ratio of quadrupole moments $^{65}Q/^{63}Q = 0.925$ as $^{65}\nu_Q = ^{63}\nu_Q(^{65}Q/^{63}Q)$.
- [11] W. Marshall and S. W. Lovesey: *Theory of Thermal Neutron Scattering* (Oxford University Press, London, 1971).
- [12] G. Shirane: *Acta Crystallogr.* **12** (1959) 282.
- [13] There is also a contribution of the valence electron to the EFG at the Cu site which is known to affect significantly the magnitude of ν_Q . However, it is expected that the symmetry of the EFG represented by η is not affected so much because the electronic orbital of the valence electron reflects the local symmetry of the site under consideration. The fact that the observed asymmetry $\eta_{\text{obs}} = 0.32$ at the Cu site agrees well with the asymmetry of the lattice EFG, $\eta_{\text{latt}} = 0.33$, evaluated by the point-charge model seems to support the above expectation.
- [14] A. J. Freeman and R. E. Watson: *Acta Crystallogr.* **14** (1961) 231.
- [15] For example, R. Kubo: *Phys. Rev.* **87** (1952) 568.
- [16] J. Kondo: *Physica B* **123** (1984) 169.
- [17] We take the positive (negative) sign of the exchange constant for the antiferromagnetic (ferromagnetic) coupling following the convention for the 1D Heisenberg spin chain with nearest-neighbor coupling $\mathcal{H} = J \sum_i \mathbf{S}_i \cdot \mathbf{S}_{i+1}$.

-
- [1] I. S. Jacobs, J. W. Bray, H. R. Hart, Jr., L. V. Interrante, J. S. Kasper, G. D. Watkins, D. E. Prober and J. C. Bonner: *Phys. Rev. B* **14** (1976) 3036.
 - [2] C. Calvo and D. Manolescu: *Acta Crystallogr.* **29** (1973) 1743.
 - [3] In the notation of ref. 2, the space group of CuV_2O_6 is $C\bar{1}$. This is an unconventional setting of $P\bar{1}$ with symmetry transforms: $x, y, z; -x, -y, -z; \frac{1}{2}+x, \frac{1}{2}+y, \frac{1}{2}+z; \frac{1}{2}-x, \frac{1}{2}-y, \frac{1}{2}-z$, yielding a C -centered triclinic cell.
 - [4] A. N. Vasil'ev, L. A. Ponomarenko, A. L. Smirnov, E. V. Antipov, Yu. A. Velikodny, M. Isobe and Y. Ueda: *Phys. Rev. B* **60** (1999) 3021.
 - [5] J. C. Bonner and M. E. Fisher: *Phys. Rev.* **135** (1964) A640.
 - [6] W. E. Hatfield: *J. Appl. Phys.* **52** (1981) 1985.